



Research articles

Study of soft magnetic composites of iron coated with nanoparticles dispersion in liquid glass

G. Tontini^{a,*}, L.L. Evangelista^a, A.I. Ramos Filho^a, R.A. Elias^b, G. Hammes^a, N.J. Batistela^b, C. Binder^a, A.N. Klein^a, V. Drago^{a,c}

^a Departamento de Engenharia Mecânica, Universidade Federal de Santa Catarina, Campus Trindade, SC, Brazil

^b Departamento de Engenharia Elétrica e Eletrônica, Universidade Federal de Santa Catarina, Campus Trindade, SC, Brazil

^c Departamento de Física, Universidade Federal de Santa Catarina, Campus Trindade, SC, Brazil



ARTICLE INFO

Keywords:

Soft magnetic composite
Sodium silicate
Magnetic power loss
Electrical resistivity
Thermogravimetric analysis

ABSTRACT

This work presents the study and development of soft magnetic composites of iron coated with alumina nanoparticles dispersed in sodium silicate, also known as liquid glass. It is proposed that the nanoparticles dispersion increases the thermal resistance of the glassy coating, allowing a heat treatment with higher temperatures, reducing the internal stresses generated during the pressing and reducing core losses. Thermogravimetric analysis under an oxidative atmosphere of the powder samples and Scanning electron microscopy and energy-dispersive X-ray diffraction of fractured compacted samples are shown to discuss the coating thermal behavior. Also, electrical resistivity, relative permeability and magnetic losses of samples with and without nanoparticles dispersed in sodium silicate are shown discussing their loss separation.

1. Introduction

Soft magnetic composite (SMC) materials are a specific class of ferromagnetic material for electromagnetic applications, composed of ferromagnetic particles insulated from each other resulting in a reduction of their eddy currents and, therefore, reducing their total energy losses [1]. Several compositions of organic and inorganic coatings were already studied and reported both in academic and patent literature like resins, phosphates, oxides, borates, deposited by a variety of methods like mechanical alloying [2], oxidizing [3,4], vapor deposition [4], wet mixture [4–6] and chemical routes [7–13].

The advantages of SMCs mainly lie in its low eddy currents, which reduces losses for medium and higher frequencies, besides its approximately isotropic nature that allows the use of different geometries for special electrical applications [1,14]. Li Y. et al., however, have shown that mechanical stress during the SMC material preparation introduces substantial magnetic anisotropy increasing considerably their rotational core losses. Coercivity is increased in the compressed direction due to changing of grain size, micro-strain of residual stress and pinning increase [15]. Even though these factors may be reduced given higher temperatures during the heat treatment [16], some of the most popular SMCs with phosphate-based coatings are processed at limited temperatures due to the degrading of their insulation properties above

typically 550 °C [17,18]. Therefore, it is still of technologic interest to develop strategies of increasing thermal resistance of insulating coatings for SMCs.

Glassy coatings, such as silicates [4,6,19–21], and boron oxide [4,12,13], represent a solution to enhance the limit of heat treatment temperature and consequently improve the magnetic performance of SMCs. These coatings also present the ability of crack healing during processing, increasing the mechanical strength and allowing for an improvement of electrical resistivity of the composite [19]. On the other hand, the combination of the viscous nature of a vitreous coating and the lacking of wettability regarding metallic surfaces may result into the outflow of the insulating layer from the interface between adjacent particles, thus increasing eddy currents losses [4]. Kloucek et al. reported the use of glass as an insulating layer of iron particles, performing pressing and heating of the insulated powder simultaneously, leading to similar strain rates of both iron and glass during processing [22]. Due to this singular processing, they were able to avoid the outflow problem, however, this solution would be very time-consuming to be applied in industry. In order to take the advantages of glassy coatings, but still keeping in mind the desirable high productivity of traditional powder metallurgy, studies are driven to improve the thermal resistance of such coatings.

This work shows the production and characterization of an SMC

* Corresponding author at: School of Materials, Faculty of Science and Engineering, The University of Manchester, Manchester, UK.

E-mail address: gustavo.tontini@manchester.ac.uk (G. Tontini).

Table 1
Iron powder composition measured by optical emission spectrometry.

Fe	Cu	S	Mn	Si	Cr	P	Ni	Sn
98.4	0.06	0.006	0.15	0.009	0.12	0.011	0.027	0.033

material composed of iron particles coated with sodium silicate and the increasing of its thermal resistance by dispersing alumina nanoparticles on the glassy coating. The samples were characterized by thermogravimetric analysis (TGA), scanning electron microscopy (SEM), energy-dispersive X-ray spectroscopy (EDX), by magnetic properties measurement performed in a Brockhaus MPG100D and electrical resistivity measurements carried with an in-house built bench.

2. Experimental

2.1. Supplies

Iron powder, from Höganäs AB Brazil, with an average particle size of 200 μm and composition presented in Table 1 were used as the ferromagnetic core for the produced SMCs.

Sodium silicate solution R2447 from Diatom and γ -alumina nanoparticles with an average size of 20 nm from Inframat Advanced Materials were used in order to produce the insulating coating of the SMC.

2.2. Sodium silicate with dispersed nanoparticles coating

For the coating of the iron powder to produce the SMC particles, the following steps were employed:

1. The sodium silicate solution was diluted in deionized water down to 5 vol%;
2. Alumina nanoparticles were sonicated within the diluted silicate solution for 5 min. The weight of alumina nanopowder was set to reach a nanoparticles concentration of 12,5 mg/ml
3. The iron powder was immersed into the previously prepared solution and stirred for 5 min;
4. The coated iron powder was magnetically separated from the remaining solution;
5. The resulting powder was dried at 80 °C for 24 h.

In order to evaluate the effect of the alumina nanoparticles on the thermal behavior of the insulating coating and on the magnetic and electrical properties, samples with and without the dispersed nanoparticles were produced according to the above-mentioned procedure. These samples were called S for samples containing only sodium silicate and S + A for samples containing sodium silicate with dispersed alumina nanoparticles.

2.3. Pressing and heat treatment

Samples based on the produced SMC powder were produced by uniaxial cold compaction, using pressing pressure of 800 MPa, followed by heat treatment carried under argon. The powder was shaped into ring samples with an outer diameter of 65 mm and a square cross section of 5×5 mm.

The heat treatment cycle aims for stress relieving as a way to decrease the hysteresis losses of the SMCs and was performed using the maximum temperatures of 500, 600 and 700 °C with a soaking time of 30 min.

The maximum temperature of the heat treatment is indicated on the samples' names being: S-500 and S + A-500 for samples treated at 500 °C; S-600 and S + A-600 for the ones treated at 600 °C; and S-700 and S + A-700 for samples treated at 700 °C. Table 2 lists the respective

Table 2
Samples densities before and after the heat treatment.

Sample	Dispersed Nanoparticles Concentration	Density (Compacted)	Heat Treatment	Density (Treated)
S-500	–	7.1 g/cm ³	500 °C	6.8 g/cm ³
S + A-500	12.5 mg/ml	7.0 g/cm ³	500 °C	6.9 g/cm ³
S-600	–	7.1 g/cm ³	600 °C	6.8 g/cm ³
S + A-600	12.5 mg/ml	7.0 g/cm ³	600 °C	7.0 g/cm ³
S-700	–	7.0 g/cm ³	700 °C	7.1 g/cm ³
S + A-700	12.5 mg/ml	6.9 g/cm ³	700 °C	7.2 g/cm ³

densities of the ring samples before and after the heat treatment.

2.4. Thermogravimetric analysis

Powder samples were prepared in the conditions of (a) uncoated iron, (b) sodium silicate coated (sample S) and (c) sodium silicate with dispersed alumina nanoparticles coated (sample S + A) for thermogravimetric analysis. These powders were analyzed in a Netzsch STA449 F3 from 50 °C up to 1150 °C under a synthetic air atmosphere with a heating rate of 10 °C/min.

2.5. Scanning electron microscopy and energy-dispersive X-ray spectroscopy

Scanning Electron Microscopy (SEM) images were obtained using a VEGA3 LMU from TESCAN with an INCAX-act energy-dispersive X-ray detector from Oxford Instruments. Microphotographs using secondary electrons detector were taken using an electron beam voltage of 15 kV and EDX color mapping images were taken for better observation of the insulating layer.

2.6. Electrical and magnetic characterization

Electrical characterization was performed on an in-house built bench that allows the contactless measurement of the electrical resistance of the same ring sample used for magnetic characterization. The use of this measurement method allows a better comprehension and correlation of the electric and magnetic results. A detailed explanation of this workbench can be found in [23].

The magnetic characterization, performed in a Brockhaus MPG100D, presented in this paper in terms of relative permeability and magnetic power losses, was carried under a sinusoidal excitation within the frequencies of 10 and 60 Hz. The measurements in these two frequencies were used for performing a simple estimation for losses separation, which allowed a better understanding of the main mechanisms of losses for each sample.

3. Results and discussion

3.1. Thermal behavior of insulating layer

The thermogravimetric analysis of the samples S and S + A are shown in Fig. 1 with a sample of the uncoated iron powder for comparison.

Notorious weight increase related to oxidation of non-coated samples can be observed in temperatures even lower than 500 °C as expected [24], while the powder coated only with sodium silicate presents oxidation signs starting at approximately 600 °C. Even higher temperatures, of nearly 700 °C, are necessary to initiate the oxidation process with an appreciable rate on the powder containing sodium silicate with dispersed alumina nanoparticles.

The TGA results show that the sodium silicate coating successfully delayed the oxidation resistance of iron powders up close to 600 °C. The observed oxidation prevention suggests that the glassy coating may act

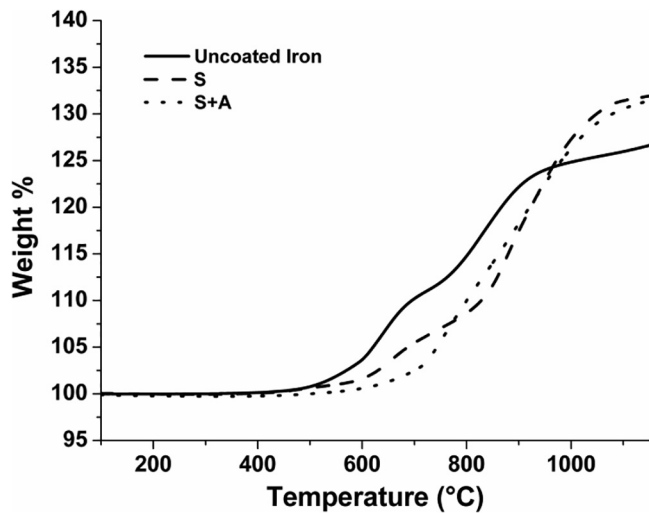


Fig. 1. Thermogravimetric analysis of samples S and S + A in comparison to uncoated iron.

as a physical barrier for oxygen diffusion, hence hindering the oxidation reaction between the iron core and atmospheric oxygen.

Further enhancement on the coating's thermal resistance (from ca. 600 °C to 700 °C) was observed in the SMC powder containing alumina nanoparticles (sample S + A). Such behavior might be related to the action of such nanoparticles as (a) thermal absorption spots, delaying the heating of the insulating layer and consequently the glass transition of sodium silicate; (b) thickening agent after the glass transition is reached, delaying the flow of the glassy insulation out of the interface between iron particles; (c) catalyst agent, accelerating the crystallization of sodium silicate and contributing to thicken even further the glassy insulation. Although further investigations are needed to determine the weight of these mechanisms on the improved behavior of the coating, a synergetic phenomenon between the nanoparticles and sodium silicate seems to be responsible for the observed enhancement of the coating thermal resistance of sample S + A.

3.2. Electrical resistivity

The measured electrical resistivity of the ring samples is presented in Fig. 2. These results show noticeably higher electrical resistivity for samples containing nanoparticles than for those without them.

A clear trend may be observed regarding the effect of temperature over the electrical resistivity. As the difference in the nature of the

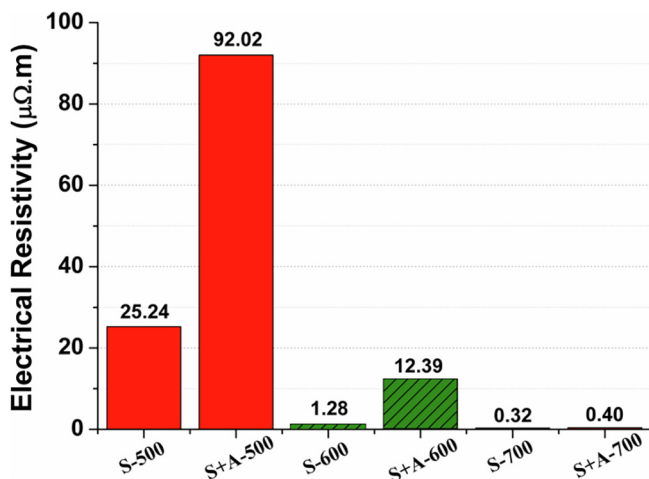


Fig. 2. Electrical resistivity of produced SMCs.

sodium silicate and the iron particle does not lead to a good wetting, the glassy silicate tends to flow out of the interface between adjacent metallic particles. This phenomenon provokes the contact between the iron particles, quickly decreasing the electrical resistivity of the SMC as the glassy silicate continues to flow out of the contact. Finally, when the heat treatment temperature is increased, the sodium silicate becomes more and more fluid, thus leading to lower and lower resistivity.

The electrical characterization results also agree with what was observed in the thermal behavior of the insulating layer. When the alumina nanoparticles are present in the insulating layer, their effects as thermal absorption spots, thickening agent and catalyst agent (as exposed in section 3.1) allow preserving, in certain levels, the electrical resistivity of the produced SMCs.

3.3. Scanning electron microscopy and energy-dispersive X-ray spectroscopy

SEM images of the fractured samples treated at 600 °C, S-600 and S + A-600, and respective EDX analysis are shown in Fig. 3. While both samples still show the coating elements over the whole iron particles, the sample S-600, without alumina nanoparticles in the glassy phase, presents an agglomeration of fiber-like structures rich in Na and O, evidencing the start of sodium silicate flow to the pores and crystallization.

3.4. Relative magnetic permeability

The relative magnetic permeability of the produced samples was measured under the frequencies of 10 and 60 Hz as presented in Fig. 4. Samples that were heat treated at higher temperatures presented higher permeability than the ones treated at lower temperatures. A trend is also observed regarding the presence or not of nanoparticles dispersed in the insulating layer, as the samples without nanoparticles also present higher permeability than the ones with them.

The effect of temperature for increasing permeability is related to two main aspects: stress relieving of iron particles, which is more effective in higher temperatures; and the outflow of the glassy insulating as previously discussed for electrical resistivity and thermogravimetric analysis. This second aspect can also be observed by the sudden decrease of permeability of sample S-700 when comparing the results from the measurements performed at 10 Hz and 60 Hz. Such reduction of the permeability with the increasing frequency is related to the counter-field generated by eddy currents. The strong appearance of this counter-field effect and the high permeability measured at 10 Hz in sample S-700 indicate that the iron particles are in intimate contact with each other.

The permeability reduction of samples containing the alumina nanoparticles may be correlated to a thicker insulating layer compared to the ones without the addition of nanoparticles. During preparation, it was noticeable that with nanoparticles the suspension became more viscous, which likely have contributed for the formation of a thicker insulating layer. This hypothesis agrees with the results of permeability decrease and resistivity increase, as for SMCs in general both presents dependence on the iron particle contact [14].

3.5. Power losses

The measured specific power losses presented in Fig. 5 were separated using the extrapolation method into static losses (Fig. 6) and dynamic losses (Fig. 7) for a better understanding of the main loss mechanism for each sample. To separate the specific losses, the method reported by Kollár P. et al was applied [25]. It consists of the measurement of the specific losses on different frequencies, extrapolating their value to frequency $f = 0$ Hz and assuming this as the static component.

Samples that were heat-treated at 700 °C present very high dynamic losses due to low electrical resistivity, even though the losses are

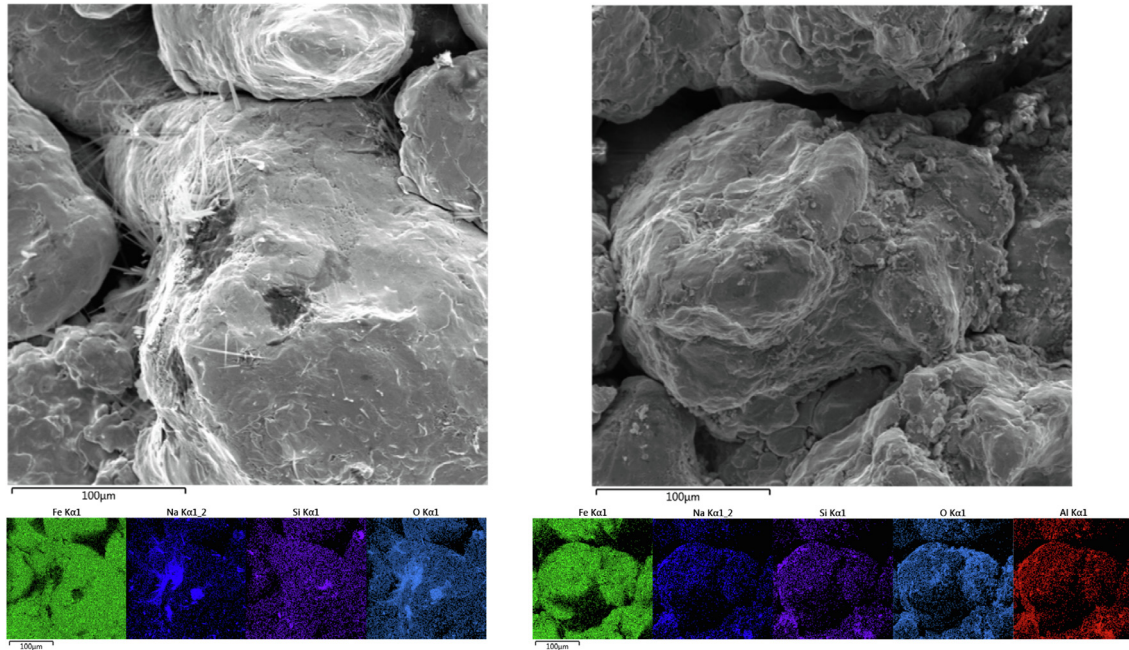


Fig. 3. Scanning electron microscopy images (top) and EDX color maps (bottom) of samples S-600 (left) and S + A-600 (right).

smaller for the sample with the insulating layer containing nanoparticles. It was initially expected that samples S-700 and S + A-700 would exhibit the lowest static losses due to the higher level of stress relieving during heat treatment at higher temperatures. However, this was not observed in the results shown in Fig. 6, which suggests that another phenomenon may be involved during the heat treatment leading to an increase of static losses for samples treated at 700 °C. Such unexpected behavior must have a deeper and focused study of the material microstructure in order to be fully understood. Furthermore, the dynamic losses results have shown that, despite nanoparticles, 30 min at 700 °C degenerates the insulation capabilities of the proposed coating.

Meanwhile, the two samples that were heat-treated at 500 °C presented nearly the same specific losses even though their static and dynamic loss components are slightly different. As the permeability has indicated regarding the insulating thickness, the non-ferromagnetic volume fraction in sample S-500 is lower than in sample S + A-500. It is well known that the non-ferromagnetic fraction act as a source of demagnetizing field [14], which may explain why sample S-500 presents

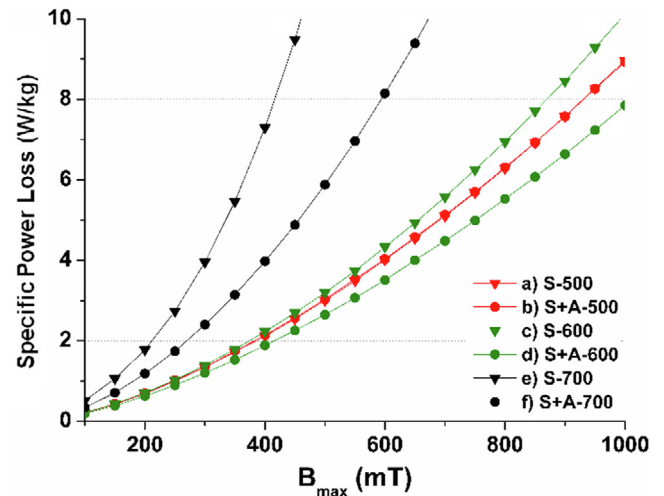


Fig. 5. Measured specific power loss of produced samples at 60 Hz.

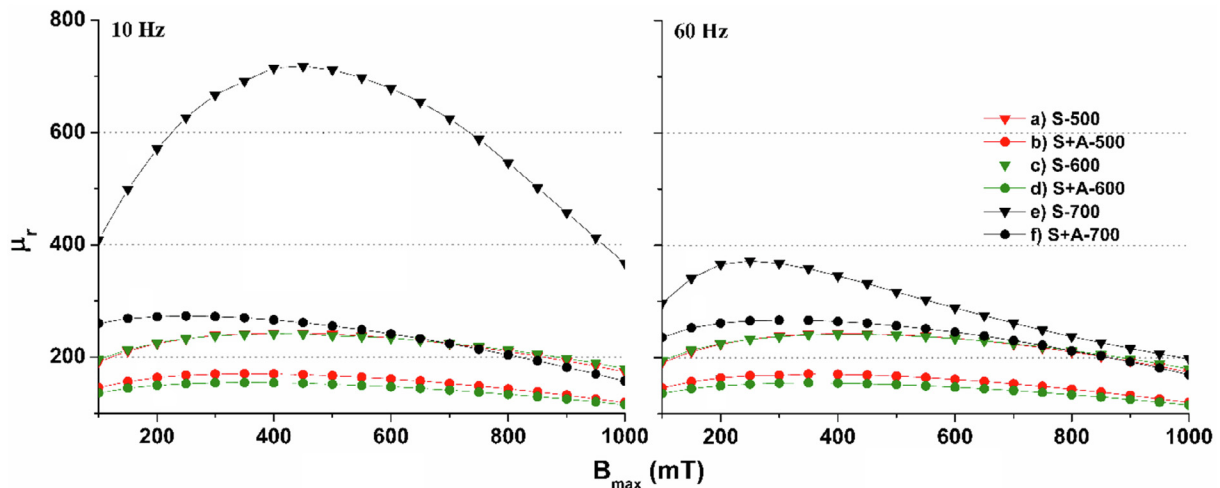


Fig. 4. Relative permeability of produced samples at 10 Hz and 60 Hz.

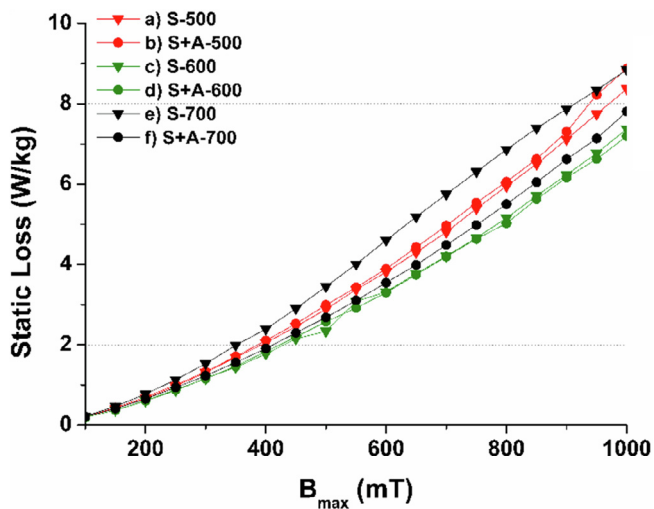


Fig. 6. Static loss of produced samples at 60 Hz.

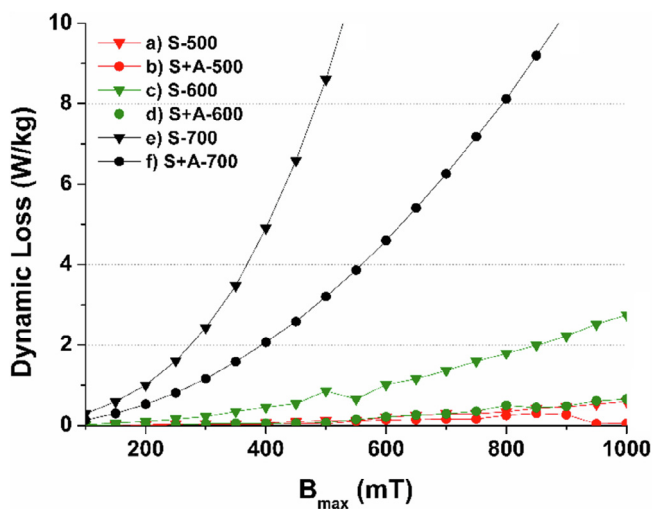


Fig. 7. Dynamic loss of produced samples at 60 Hz.

lower static losses than S + A-500. On the other hand, the thicker insulating coating of sample S + A-500 leads to higher electrical resistivity and consequently lower dynamic losses when compared to sample S-500.

Finally, the samples treated at 600 °C presented the lowest static losses with very small differences between the samples with and without nanoparticles. However, the dynamic losses of sample S + A-600 are much smaller than the ones obtained for sample S-600, which agree with the previous results of electrical resistivity. That causes the sample S + A-600 to be one with the lowest losses obtained in this study. This result also emphasizes the important role of alumina nanoparticles for obtaining an insulating coating that can support higher temperatures in order to minimize the static losses while keeping dynamic losses at an acceptable level.

4. Conclusions

Alumina nanoparticles have successfully demonstrated the ability to enhance the thermal resistance of a sodium silicate coating, which leads to SMCs with improved electric and magnetic properties.

The addition of the nanoparticles delays the outflow of sodium silicate from the interface between adjacent particles as demonstrated by TGA in an oxidative atmosphere. That effect has contributed for the coating to keep higher electrical resistivity even when heat treatment

occurred in temperatures higher than usual.

The nanoparticles also have thickened the suspension used for coating the iron particles, producing a thicker insulating layer. The thickness difference between the samples with and without the nanoparticles was observed indirectly in the results of relative permeability. For further optimization of the proposed SMC, the coating thickness may be controlled by adjusting the concentration of alumina nanoparticles in the initial suspension.

Additionally, the power losses results indicate that the addition of alumina nanoparticles dispersed in sodium silicate allowed for heat treatment temperatures of the proposed SMC up to 600 °C. This higher temperature enhanced the stress relieving of the tested SMC while keeping the electrical resistivity high enough to maintain a low level of dynamic losses. The results showed that without the nanoparticles the temperature of 600 °C, although reducing static losses, would be too deleterious for dynamic losses. That comparison emphasizes the important role that the alumina nanoparticles played for enhancing the thermal resistance of the glassy coatings in order to improve the properties of an SMC material.

Nevertheless, in order to use the SMC studied in this work in an industrial application, it is necessary to perform an investigation not only of the mechanical properties but over the coefficient of thermal expansion of both iron particles and the glassy coatings as SMCs do not typically operate at room temperature.

Acknowledgements

We thank Brazilian Agencies CAPES, CNPq, BNDES and FEESC, and Brazilian Company EMBRACO, for their financial support.

Research supported by LABMAT-UFSC, GRUCAD-UFSC and PGMAT-UFSC.

References

- [1] H. Shokrollahi, K. Janghorban, Soft magnetic composite materials (SMCs), *J. Mater. Process. Technol.* 189 (2007) 1–12, <https://doi.org/10.1016/j.jmatprotec.2007.02.034>.
- [2] K.J. Sunday, K.A. Darling, F.G. Hanejko, B. Anasori, Y.-C. Liu, M.L. Taheri, Al₂O₃ “self-coated” iron powder composites via mechanical milling, *J. Alloys Compd.* 653 (2015) 61–68, <https://doi.org/10.1016/J.JALLCOM.2015.08.260>.
- [3] L. Qian, J. Peng, Z. Xiang, Y. Pan, W. Lu, Effect of annealing on magnetic properties of Fe/Fe₃O₄ soft magnetic composites prepared by in-situ oxidation and hydrogen reduction methods, *J. Alloys Compd.* 778 (2019) 712–720, <https://doi.org/10.1016/J.JALLCOM.2018.11.184>.
- [4] M.V.F. da Luz, R. Carlson, N. Sadowski, G. Hammes, V. Drago, G. Tontini, A.N. Klein, C. Binder, J.B. Rodrigues Neto, N.J. Batistela, M.T. Daros, A.I. Ramos Filho, C. Schmitz, R.D.A. Elias, Ferromagnetic particle surface coating layers for obtaining soft magnetic composites (smcs), WO2018035595A1 (2018), <https://patents.google.com/patent/WO2018035595A1/en>.
- [5] T. Gheiratmand, H.R. Madaah Hosseini, S.M. Seyed Reihani, Iron-borosilicate soft magnetic composites: the correlation between processing parameters and magnetic properties for high frequency applications, *J. Magn. Magn. Mater.* (2017), <https://doi.org/10.1016/j.jmmm.2017.01.047>.
- [6] A. Watanabe, T. Maeda, T. Ueno, T. Ishimine, Soft magnetic powder, granulated powder, dust core, electromagnetic component, and method for producing dust core, US20130181802A1 (2013).
- [7] K.J. Sunday, M.L. Taheri, NiZnCu-ferrite coated iron powder for soft magnetic composite applications, *J. Magn. Magn. Mater.* 463 (2018) 1–6, <https://doi.org/10.1016/J.JMMM.2018.05.030>.
- [8] J. Lei, J. Zheng, H. Zheng, L. Qiao, Y. Ying, W. Cai, W. Li, J. Yu, M. Lin, S. Che, Effects of heat treatment and lubricant on magnetic properties of iron-based soft magnetic composites with Al₂O₃ insulating layer by one-pot synthesis method, *J. Magn. Magn. Mater.* 472 (2019) 7–13, <https://doi.org/10.1016/J.JMMM.2018.09.125>.
- [9] C. Xia, Y. Peng, Y. Yi, H. Deng, Y. Zhu, G. Hu, The magnetic properties and microstructure of phosphated amorphous FeSiCr/silane soft magnetic composite, *J. Magn. Magn. Mater.* 474 (2019) 424–433, <https://doi.org/10.1016/J.JMMM.2018.11.058>.
- [10] Z. Chen, X. Liu, X. Kan, Z. Wang, R. Zhu, W. Yang, Q. Wu, M. Shezad, Phosphate coatings evolution study and effects of ultrasonic on soft magnetic properties of FeSiAl by aqueous phosphoric acid solution passivation, *J. Alloys Compd.* 783 (2019) 434–440, <https://doi.org/10.1016/J.JALLCOM.2018.12.328>.
- [11] Y. Yi, Y. Peng, C. Xia, L. Wu, X. Ke, J. Nie, Influence of heat treatment on microstructures and magnetic properties of Fe-based soft magnetic composites prepared by co-precipitation method, *J. Magn. Magn. Mater.* 476 (2019) 100–105, <https://doi.org/10.1016/J.JMMM.2018.11.058>.

- doi.org/10.1016/J.JMMM.2018.12.049.
- [12] G. Vachon, C. Gelinas, Insulated iron-base powder for soft magnetic applications, US8911663B2, 2014. <https://patents.google.com/patent/US8911663B2/en>.
- [13] L. Liya, Y. Jianhong, L. Aikun, W. Longwen, A soft-magnetic composite powder and preparation method, CN 103177838 B, 2016. <https://www.google.com/patents/CN103177838B?cl=en>.
- [14] E.A. Périgo, B. Weidenfeller, P. Kollár, J. Füzer, Past, present, and future of soft magnetic composites, Appl. Phys. Rev. 5 (2018) 031301, <https://doi.org/10.1063/1.5027045>.
- [15] Yongjian Li, Yafeng Liu, Fugui Liu, Qingxin Yang, Pengxiang Ren, Magnetic anisotropic properties measurement and analysis of the soft magnetic composite materials, IEEE Trans. Appl. Supercond. 24 (2014) 1–4, <https://doi.org/10.1109/TASC.2014.2348569>.
- [16] A. Hossein Taghvaei, A. Ebrahimi, K. Gheisari, K. Janghorban, Analysis of the magnetic losses in iron-based soft magnetic composites with MgO insulation produced by sol–gel method, J. Magn. Magn. Mater. 322 (2010) 3748–3754, <https://doi.org/10.1016/J.JMMM.2010.07.032>.
- [17] B. Ślusarek, J. Szczygłowski, K. Chwastek, B. Jankowski, The effects of excitation conditions and annealing temperature on power loss in SMC cores, Prz. Elektrotechniczny. 4 (2015) 16–21 (accessed May 12, 2015), http://www.researchgate.net/publication/274321182_The_effects_of_excitation_conditions_and_annealing_temperature_on_power_loss_in_SMC_cores.
- [18] L.L. Evangelista, D.S. Avila, M.A. Carvalho, H.D. Lopes, P.A.P. Wendhausen, Mechanical strength and energy losses optimization of somaloy 3P 700-based components, IEEE Trans. Magn. 52 (2016) 5–8, <https://doi.org/10.1109/TMAG.2016.2516964>.
- [19] W. Ding, L. Jiang, Y. Liao, J. Song, B. Li, G. Wu, Effect of iron particle size and volume fraction on the magnetic properties of Fe/silicate glass soft magnetic composites, J. Magn. Magn. Mater. 378 (2015) 232–238, <https://doi.org/10.1016/J.JMMM.2014.09.019>.
- [20] W. Ding, L. Jiang, B. Li, G. Chen, S. Tian, G. Wu, Microstructure and magnetic properties of soft magnetic composites with silicate glass insulation layers, J. Supercond. Nov. Magn. 27 (2014) 239–245, <https://doi.org/10.1007/s10948-013-2249-6>.
- [21] T. Gheiratmand, H.R. Madaah Hosseini, F. Shalbaf, M. Mohhebbali, M.A. Mozaffari, S.H. Arabi, F. Farzanegan, Effect of iron particles size on the high-frequency magnetic properties of iron-borosilicate soft magnetic composites, J. Supercond. Nov. Magn. (2017) 1–6, <https://doi.org/10.1007/s10948-017-4115-4>.
- [22] F. Kloucek, C. Schüller, U. Feller, Soft magnetic metal-glass composite material with low eddy current losses, J. Phys. Colloq. C 6 (1985) 197–202, <https://doi.org/10.1051/jphyscol:1985634>.
- [23] I. Pitta, R.D.A. Elias, B.J. Mailhé, F.M. Cardenuto, N. Jhoe, N. Sadowski, J.V. Leite, Ring shaped ferromagnetic samples resistivity measurement, 18 SBMO – Simpósio Bras. Microondas e Optoeletrônica e 13 CBMAG – Congr. Bras. Eletromagnetismo Ring, 2018, pp. 697–701.
- [24] N. Bertrand, C. Desgranges, D. Poquillon, M.C. Lafont, D. Monceau, Iron Oxidation at low temperature (260–500 °C) in air and the effect of water vapor, Oxid. Met. 73 (2010) 139–162, <https://doi.org/10.1007/s11085-009-9171-0>.
- [25] P. Kollár, Z. Birčáková, J. Füzer, R. Bureš, M. Fáberová, Power loss separation in Fe-based composite materials, J. Magn. Magn. Mater. 327 (2013) 146–150, <https://doi.org/10.1016/j.jmmm.2012.09.055>.